

# Temporal artifact minimization in sonoelastography through optimal selection of imaging parameters (L)

Gabriela Torres,<sup>1</sup> Gustavo R. Chau,<sup>1</sup> Kevin J. Parker,<sup>2</sup> Benjamin Castaneda,<sup>1</sup> and Roberto J. Lavarello<sup>1,a)</sup>

<sup>1</sup>Laboratorio de Imágenes Médicas, Departamento de Ingeniería, Pontificia Universidad Católica del Perú, Lima 32, Peru

<sup>2</sup>Electrical and Computer Engineering Department, University of Rochester, Rochester, New York 14627, USA

(Received 9 December 2015; revised 22 June 2016; accepted 1 July 2016; published online 28 July 2016)

Sonoelastography is an ultrasonic technique that uses Kasai's autocorrelation algorithms to generate qualitative images of tissue elasticity using external mechanical vibrations. In the absence of synchronization between the mechanical vibration device and the ultrasound system, the random initial phase and finite ensemble length of the data packets result in temporal artifacts in the sonoelastography frames and, consequently, in degraded image quality. In this work, the analytic derivation of an optimal selection of acquisition parameters (i.e., pulse repetition frequency, vibration frequency, and ensemble length) is developed in order to minimize these artifacts, thereby eliminating the need for complex device synchronization. The proposed rule was verified through experiments with heterogeneous phantoms, where the use of optimally selected parameters increased the average contrast-to-noise ratio (CNR) by more than 200% and reduced the CNR standard deviation by 400% when compared to the use of arbitrarily selected imaging parameters. Therefore, the results suggest that the rule for specific selection of acquisition parameters becomes an important tool for producing high quality sonoelastography images. © 2016 Acoustical Society of America.

[<http://dx.doi.org/10.1121/1.4958997>]

[KAW]

Pages: 714–717

## I. INTRODUCTION

Ultrasonic techniques enable the estimation of tissue properties using various imaging approaches. In particular, sonoelastography enables the estimation of elasticity using external mechanical sources to induce sinusoidal vibrations in the analyzed medium. This technique is based on the linear relationship between the displacement of vibrating scatterers and the spread of the Doppler spectrum.<sup>1</sup> The spectral variance for Doppler imaging is usually obtained using Kasai's autocorrelation estimator (KAE).<sup>2</sup>

Typically, the external vibrating sources and the ultrasound scanner used in a sonoelastography experiment are not synchronized. As a result, each Doppler packet corresponds, in general, to a different fragment of the vibration signal, resulting in random initial phases. Unfortunately, this condition may create issues when estimating the Doppler spread using the Doppler modes currently available in ultrasound scanners. In particular, previous publications have shown that the KAE's performance is dependent on the parameters used for data acquisition<sup>3</sup> and it is influenced by discrete-time signals and finite-sized ensemble lengths.<sup>4</sup> The random variation in the initial phase of the Doppler packets translates into variations of the estimated Doppler spread. As a result, pixel brightness on the sonoelastography maps suffers

from temporal artifacts where the estimated value changes as the initial phase of the packet varies.

There are many potential solutions to eliminate this problem, including synchronizing the mechanical vibrators and the ultrasound scanner so that each packet has the same initial phase, post-processing the data by using interpolation and phase rotation methods, and using other motion detection algorithms less sensitive to the initial phase problem. However, these solutions require either direct access to the raw data or performing software or hardware modifications to the scanner. In contrast, an alternative solution was recently proposed which only requires the selection of specific values of particular acquisition parameters (i.e., pulse repetition frequency, ensemble length, and vibration frequency).<sup>5</sup> The rule for selecting these parameters, however, was empirically derived based on a limited set of simulations and experimental results in homogeneous media. This work presents the analytic derivation of the proposed rule in order to establish a formal generalization for all the possible combinations of scanning parameters, and further demonstrates the validity and usefulness of the proposed rule by presenting experimental results when imaging inhomogeneous media.

## II. THEORY

In sonoelastography, all scatterers move at a vibration frequency  $f_v$  and with a displacement amplitude  $A$  which is related to the material elasticity. Given a mechanical

<sup>a)</sup>Electronic mail: [lavarello.rj@pucp.edu.pe](mailto:lavarello.rj@pucp.edu.pe)

sinusoidal vibration, the variation in arrival time of the back-scattered echoes in the  $n$ th frame can be expressed as

$$\Delta t_n = A \sin(2\pi f_v n T_{\text{PRF}} + \varphi), \quad n = 0, \dots, N-1, \quad (1)$$

where  $\varphi$  is the initial phase of the ensemble,  $N$  is the ensemble length, PRF is the pulse repetition frequency, and  $T_{\text{PRF}} = 1/\text{PRF}$  is the pulse repetition period. Based on the typical assumptions of Doppler imaging, if the modeled signal is narrowband and  $\Delta t_n \ll 2\pi/\omega_0$  (where  $\omega_0$  is the transducer's center frequency), the signal for each ensemble can be written as

$$s_n(t) = s(t)e^{-i\omega_0 \Delta t_n}, \quad (2)$$

where  $s(t)$  is the received backscattered signal. Before the application of the Kasai estimation algorithm, a wall filter (WF) is applied to the acquired signal. In this work, a WF of length  $P$  will be assumed in accordance with typically available filters in ultrasound scanners. In this case, the WF is employed to increase the sensitivity of the system to the measurement of low-amplitude vibrations (i.e., 5 to 20  $\mu\text{m}$ ). The filtered signal can therefore be expressed as

$$\begin{aligned} s_n^{\text{WF}}(t) &= \sum_{m=1}^P \alpha_m s_{n-m}(t) \\ &= s(t) \sum_{m=1}^P \alpha_m e^{-i\omega_0 \Delta t_{n-m}}, \end{aligned} \quad (3)$$

where  $\alpha_m$  is the WF  $m$ th coefficient. The Doppler variance is estimated as<sup>2</sup>

$$\sigma^2 = \frac{2}{T_{\text{PRF}}^2} \left( 1 - \frac{|R(1)|}{|R(0)|} \right), \quad (4)$$

$$R(0) = \sum_{n=1}^{N-P} s_n^{\text{WF}}(t) (s_n^{\text{WF}}(t))^*, \quad (5)$$

$$R(1) = \sum_{n=1}^{N-P} s_{n+1}^{\text{WF}}(t) (s_n^{\text{WF}}(t))^*. \quad (6)$$

By combining Eqs. (3) and (5),  $R(0)$  can be written as

$$\begin{aligned} R(0) &= |s(t)|^2 \sum_{n=1}^{N-P} \left[ \left( \sum_{m=1}^P \alpha_m e^{-i\omega_0 \Delta t_{n-m}} \right) \right. \\ &\quad \left. \times \left( \sum_{m'=1}^P \alpha_{m'} e^{i\omega_0 \Delta t_{n-m'}} \right) \right]. \end{aligned} \quad (7)$$

The expression above can be expanded as

$$\begin{aligned} R(0) &= |s(t)|^2 \sum_{n=1}^{N-P} \left[ \sum_{m=m'}^P \alpha_m^2 \right. \\ &\quad \left. + \sum_{m=1}^P \sum_{\substack{m'=1 \\ m \neq m'}}^P \alpha_m \alpha_{m'} e^{-i\omega_0 \Delta t_{n-m}} e^{i\omega_0 \Delta t_{n-m'}} \right]. \end{aligned} \quad (8)$$

Using the identity<sup>1</sup>

$$e^{i\beta \sin \alpha} = \sum_{n=-\infty}^{\infty} J_n(\beta) e^{in\alpha}, \quad (9)$$

where  $J_n$  is the  $n$ th order Bessel function of the first kind. This term can be written as

$$\begin{aligned} R(0) &= |s(t)|^2 \sum_{n=1}^{N-P} \left[ \sum_{m=m'}^P \alpha_m^2 + \sum_{\substack{m=1 \\ m \neq m'}}^P \sum_{m'=1}^P \alpha_m \alpha_{m'} \right. \\ &\quad \left. \times \sum_k J_k(\omega_0 A) e^{-ik\Delta\varphi_{n-m}} \sum_h J_h(\omega_0 A) e^{ih\Delta\varphi_{n-m'}} \right]. \end{aligned} \quad (10)$$

Therefore, it can be expressed as

$$\begin{aligned} R(0) &= |s(t)|^2 \left( \sum_{m=m'}^P \alpha_m^2 \right) (N-P) + |s(t)|^2 \\ &\quad \times \sum_{\substack{m=1 \\ m \neq m'}}^P \sum_{m'=1}^P \alpha_m \alpha_{m'} \sum_{k=h} J_k^2(\omega_0 A) e^{ik2\pi f_v T_{\text{PRF}}(m-m')} (N-P) \\ &\quad + |s(t)|^2 \sum_{\substack{m=1 \\ m \neq m'}}^P \sum_{m'=1}^P \alpha_m \alpha_{m'} \sum_k \sum_{\substack{h \\ k \neq h}} J_k(\omega_0 A) J_h(\omega_0 A) \\ &\quad \times \sum_{n=1}^{N-P} \psi \zeta e^{-i2\pi f_v T_{\text{PRF}}(hm'-km)}, \end{aligned} \quad (11)$$

where

$$\zeta = \sum_{n=1}^{N-P} e^{i2\pi f_v n T_{\text{PRF}}(k-h)} \quad (12)$$

and

$$\psi = e^{i2\pi f_v T_{\text{PRF}}(h-k)\varphi}. \quad (13)$$

Similarly,  $R(1)$  can be written as

$$\begin{aligned} R(1) &= |s(t)|^2 \sum_{n=1}^{N-P} \left[ \left( \sum_{m=1}^P \alpha_m e^{-i\omega_0 \Delta t_{n-m+1}} \right) \right. \\ &\quad \left. \times \left( \sum_{m'=1}^P \alpha_{m'} e^{i\omega_0 \Delta t_{n-m'}} \right) \right]. \end{aligned} \quad (14)$$

Using Eq. (9), Eq. (14) can be expanded as

$$\begin{aligned} R(1) &= |s(t)|^2 \sum_{n=1}^{N-P} \left[ \sum_{m=1}^P \alpha_m^2 \right. \\ &\quad \left. + \sum_{\substack{m=1 \\ m \neq m'}}^P \sum_{m'=1}^P \alpha_m \alpha_{m'} \sum_k J_k(\omega_0 A) e^{-ik\Delta\varphi_{n-m+1}} \right. \\ &\quad \left. \times \sum_h J_h(\omega_0 A) e^{ih\Delta\varphi_{n-m'}} \right]. \end{aligned} \quad (15)$$

Expanding and reordering the terms results in

$$\begin{aligned}
R(1) &= |s(t)|^2 \left( \sum_{m=1}^P \sum_{m'=1}^P \alpha_m \alpha_{m'} \right) (N - P) \\
&+ |s(t)|^2 \sum_{\substack{m=1 \\ m \neq m'}}^P \sum_{\substack{m'=1 \\ m' \neq m}}^P \alpha_m \alpha_{m'} \sum_{k=h}^P J_k^2(\omega_0 A) (N - P) \\
&\times e^{ik2\pi f_v T_{\text{PRF}}(m-m'-1)} \\
&+ |s(t)|^2 \sum_{\substack{m=1 \\ m \neq m'}}^P \sum_{\substack{m'=1 \\ m' \neq m}}^P \alpha_m \alpha_{m'} \sum_{k=h}^P \sum_{h}^P J_k(\omega_0 A) \psi \xi \\
&\times e^{-i2\pi f_v T_{\text{PRF}}[hm'-k(m-1)]}. \tag{16}
\end{aligned}$$

From Eqs. (11) and (16), the factor  $\psi$  is the only term dependent on  $\varphi$ . However, by properly choosing the imaging parameters, the sum in  $\xi$  can vanish thereby canceling the effects of  $\psi$  in the calculation of the autocorrelation terms. In particular, if  $f_v$ ,  $N$ ,  $P$ , and PRF are chosen such that

$$\frac{f_v(N - P)}{\text{PRF}} = l, \tag{17}$$

where  $l$  is any arbitrary positive integer. Then,

$$\sum_{n=1}^{N-P} e^{i2\pi f_v n T_{\text{PRF}}(h-k)} = 0, \quad k \neq h. \tag{18}$$

Therefore, the proposed combination of scanning parameters eliminates the initial  $\varphi$  phase dependence of the KAE. A key result derived from Eq. (17) is that selecting PRF as a multiple of  $f_v$  is not a sufficient condition for reducing temporal artifacts in sonoelastography, but also a proper selection of the ensemble length  $N$  is needed. As a result, the parameter selection rule in Eq. (17) avoids the generation of artifacts in sonoelastographic images without the need for synchronization between the vibrators and the ultrasonic scanner.

### III. EXPERIMENTS

The effectiveness of the proposed combination of scanning parameters was experimentally verified. A 4040B signal generator (B&K Precision Corp., Yorba Linda, CA) and an A-X500 amplifier (TEAC, Tokyo, Japan) were connected to a 4810 mechanical vibrator (Brüel & Kjær, Nærum, Denmark) located on one side of a heterogeneous phantom. For these experiments, a LOGIQ 9 ultrasound scanner (GE Healthcare, Milwaukee, WI) was used for scanning and acquiring colorflow data with a frame rate of 12 Hz, using an M12L linear array ultrasound transducer (GE Healthcare, Wauwatosa, WI) with a transmit frequency of 5 MHz and a sampling rate of the IQ data of 10 MHz.

Two phantoms made with 300 bloom pork gelatin (Gelatin Innovations, Addison, IL) were prepared using the same procedure as Hah *et al.*<sup>6</sup> The first phantom was prepared with a 10% gelatin background and one 16% gelatin cylindrical inclusion with 10 mm radius. The second one was prepared as a homogeneous mixture with 10% gelatin. The first phantom was used to evaluate the ability to detect

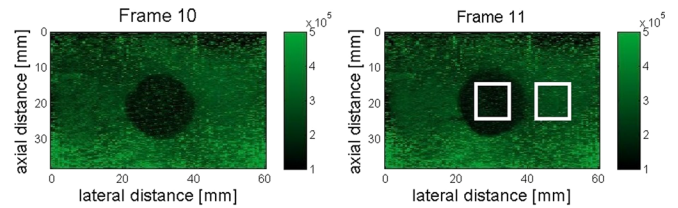


FIG. 1. (Color online) Sonoelastographic results with optimized parameters (expressed in  $\text{Hz}^2$ ) for two frames of an inhomogeneous phantom (hard lesion inclusion—near center) using a LOGIQ 9 scanner with  $f_v = 200$  Hz, PRF = 600 Hz,  $P = 2$ , and  $N = 14$ .

the inclusion using the contrast-to-noise ratio (CNR), calculated as

$$\text{CNR} = \frac{|\mu_i - \mu_b|}{\sqrt{\sigma_i^2 + \sigma_b^2}}, \tag{19}$$

where  $\mu$  and  $\sigma^2$  are the mean and variance of the sonoelastography values, respectively, and the subscripts  $b$  and  $i$  refer to the background and inclusion regions, respectively. The performance was quantified for the total of 28 frames in the sonoelastography videos corresponding to the frames shown in Figs. 1 and 2. All calculations were performed considering  $10 \times 10$  mm regions within the background and inclusion as depicted in Fig. 1. The second phantom was used for evaluating parameter selections for vibration frequencies in the range of 100 to 300 Hz. For these results, the coefficient of variation was calculated as

$$\text{Coefficient of variation} = \frac{\sigma}{\mu}, \tag{20}$$

where  $\sigma$  and  $\mu$  represent the standard deviation and the mean, respectively, of a  $20 \times 20$  mm region located at the center of the elastogram.

Figures 1 and 2 illustrate how the sonoelastograms are affected by temporal artifacts. The sonoelastographic frames in Fig. 1 correspond to a set of parameters that follow Eq. (17), i.e.,  $N = 14$ ,  $P = 2$ ,  $f_v = 200$  Hz, and PRF = 600 Hz, and therefore temporal artifacts are not observed as evidenced by the high correlation among images in different frames. Moreover, both frames 10 and 11 present a clear difference between the inclusion and background. In contrast, the frames in Fig. 2 are affected by artifacts as the imaging parameters do not follow Eq. (17), i.e.,  $N = 12$ ,  $P = 2$ ,  $f_v = 200$  Hz, and PRF = 600 Hz.

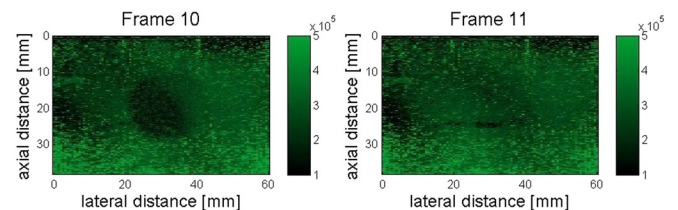


FIG. 2. (Color online) Sonoelastographic results without optimized parameters (expressed in  $\text{Hz}^2$ ) for two frames of an inhomogeneous phantom (hard lesion inclusion—near center) using a LOGIQ 9 scanner with  $f_v = 200$  Hz, PRF = 600 Hz,  $P = 2$ , and  $N = 12$ .

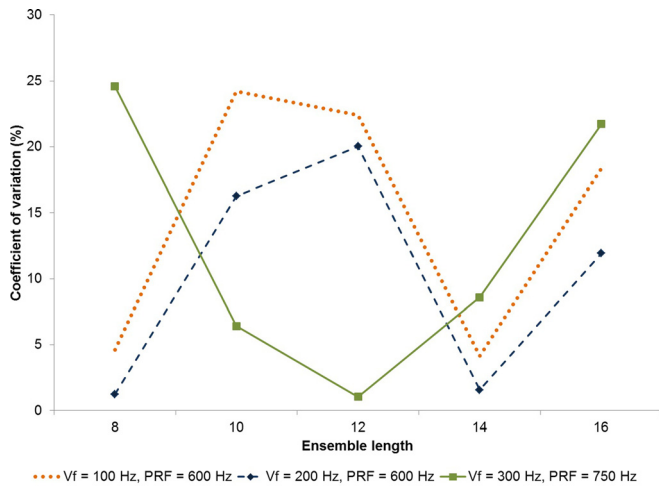


FIG. 3. (Color online) Coefficient of variation for experiments with a homogeneous phantom using the available ensemble length range from  $N=8$  to  $N=16$ , using  $P=2$ , with combinations of  $f_v=100$  Hz and PRF = 600 Hz (dotted line),  $f_v=200$  Hz and PRF = 600 Hz (dashed line), and  $f_v=300$  Hz and PRF = 750 Hz (solid line).

This is evidenced by the reduced visualization of the inclusion in frame 11 when compared to frame 10.

Figure 3 shows the experimental results obtained using the homogeneous phantom. In this case, three combinations of  $f_v$  and PRF were used for five ensemble lengths. These results demonstrate how the parameter selection affects the results for three vibration frequencies: 100, 200, and 300 Hz.

#### IV. DISCUSSION

The selection of scanning parameters in this study is presented to guide end-users with commercial Doppler scanning devices to create and optimize sonoelasticity images without the need of synchronization, post-processing, or beamforming alterations. In this context, this selection provides a potential alternative when using widely available Doppler scanners, including small portable devices.

It can be observed in Fig. 4 that the use of the proposed rule for selecting imaging parameters resulted in a 227% increase in average CNR when compared to the case of arbitrarily selected parameters (i.e.,  $\mu_{\text{CNR}}$  from 0.91 to 2.07). In fact, theoretically, as the regions are not changing, the frames should maintain a constant CNR over time. It can be observed that the case that most approximates to this behavior is given by the parameter combination with ensemble length 14, proving that KAE is dependent of three parameters:  $f_v$ , PRF, and  $N$ . Additionally, when selecting different combinations of parameters, the CNR varied up to 400% between different frames per acquisition. It can be observed that the difference between the maximum and minimum values of CNR was of 1.28 for  $N=12$  and 0.42 for  $N=14$ , illustrating how the presence of artifacts generated quantifiable distortions in sonoelastography imaging.

Furthermore, results using the homogeneous phantom (see Fig. 3) demonstrate that for the analyzed frequencies, only the parameter combinations that followed the proposed rule provided a coefficient of variation lower than 5% using a two-point WF. In the case of  $f_v=100$  Hz and PRF = 600 Hz,

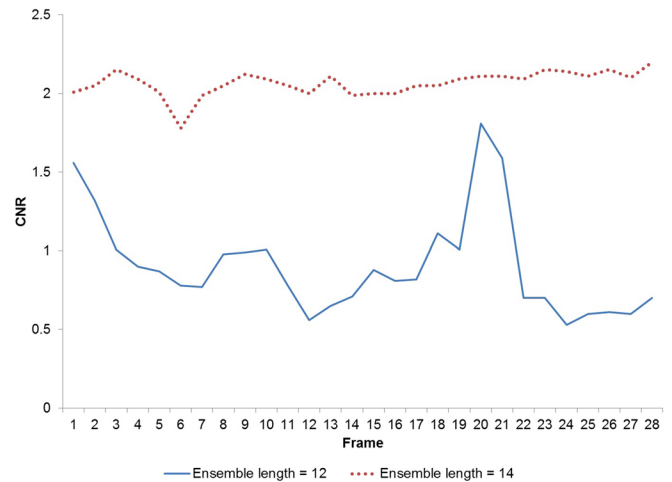


FIG. 4. (Color online) Mean CNR for each sonoelastography frame using  $f_v=200$  Hz, PRF = 600 Hz,  $P=2$ , and ensemble lengths  $N$  of 12 (solid line) and 14 (dotted line).

ensemble lengths of 8 and 14 provided the lowest coefficient of variations. The two ensemble lengths also accomplish these results when  $f_v$  is doubled, as this also follows Eq. (17). Moreover, in the case of  $f_v=300$  Hz and PRF = 750 Hz, only an ensemble length of 12 satisfies Eq. (17) and provides a coefficient of variation of less than 5%.

#### V. CONCLUSIONS

The analytic derivation of a rule for selecting imaging parameters for sonoelastography was presented, as an alternative to synchronization. The initial phase dependence of the Kasai's autocorrelation algorithm was reduced and results were verified with experiments. For tests with inhomogeneous phantoms, when the selection of imaging parameters followed the proposed rule, the CNR was increased by 400% in comparison to arbitrary parameters selection.

#### ACKNOWLEDGMENTS

Research supported by Grants 205-FINCYT-IA-2013 and 012-2014-FONDECYT-C1 from the Peruvian Government.

- <sup>1</sup>S. Huang, R. M. Lerner, and K. J. Parker, "On estimating the amplitude of harmonic vibration from the Doppler spectrum of reflected signals," *J. Acoust. Soc. Am.* **88**, 2702–2712 (1990).
- <sup>2</sup>C. Kasai, K. Namekawa, A. Koyano, and R. Omoto, "Real-time two-dimensional blood flow imaging using an autocorrelation technique," *IEEE Trans. Sonics Ultrasonics* **32**, 458–464 (1985).
- <sup>3</sup>A. Chan, E. Lam, and V. Srinivasan, "Comparison of Kasai autocorrelation and maximum likelihood estimators for Doppler optical coherence tomography," *IEEE Trans. Med. Imag.* **32**, 1033–1042 (2013).
- <sup>4</sup>S. Huang, R. M. Lerner, and K. J. Parker, "Time domain Doppler estimators of the amplitude of vibrating targets," *J. Acoust. Soc. Am.* **91**, 965–974 (1992).
- <sup>5</sup>G. Torres, J. Ormachea, R. J. Lavarello, K. J. Parker, and B. Castaneda, "Effects of data acquisition parameters on the quality of sonoelastographic imaging," in *37th Annual International Conference of the IEEE Engineering in Medicine and Biology Society (EMBC)*, 2015, pp. 3839–3842.
- <sup>6</sup>Z. Hah, C. Hazard, B. Mills, C. Barry, D. Rubens, and K. Parker, "Integration of crawling waves in an ultrasound imaging system. Part 2: Signal processing and applications," *Ultrasound Med. Biol.* **38**, 312–323 (2012).